

RANGES AND CRITICAL VALUES OF ADVANCE RATIO
FOR BLADE/VORTEX INTERSECTION PATTERNS OF A HELICOPTER ROTOR

by
L.R. Lucassen

FIFTH EUROPEAN ROTORCRAFT AND POWERED LIFT AIRCRAFT FORUM
SEPTEMBER 4 – 7 TH 1979 - AMSTERDAM, THE NETHERLANDS

SUMMARY

The free vortices trailing from the tip of helicopter rotor blades lead to large changes in induced velocity and local angle of attack, resulting in peaks in aerodynamic loading. For a single rotor in forward flight an analysis has been performed on the geometry of blade/vortex intersection, while an undistorted, in-plane wake is assumed. This showed the existence of seven ranges of advance ratio, each range being characterized by a different blade/vortex intersection pattern. These ranges are separated by six critical advance ratios, which are functions only of the ratio between the number of rotor blades and the serial number (index) of the preceding blade or tip vortex.

The lowest critical advance ratio is in agreement with data published by HILL on the position of a ripple in the power-required curves for level flight, as measured by the Naval Air Test Center for several helicopter types.

CONTENTS

	page
LIST OF SYMBOLS	2
1 INTRODUCTION	3
2 ASSUMPTIONS	3
3 BLADE-ELEMENT PATH	5
3.1 Arbitrary blade element	5
3.2 Tip element and tip vortex	5
4 TIP-VORTEX PATTERN OF A ROTOR	7
5 BLADE/TIP-VORTEX INTERSECTION	7
5.1 Main parameters	7
5.2 Derivation of intersection formula	7
5.3 Particular ψ - and x -values	8
5.4 Blade/vortex angle	8
5.5 Numerical results	10
6 DISCUSSION	10
6.1 Common characteristics of intersection	10
6.2 Main advance-ratio ranges	10
6.3 Common characteristics of μ -ranges 1 and 2	11
6.3.1 Minimum radius	11
6.3.2 Tip intersection on rear side	12
6.3.3 Radial tangent	12
6.4 Advance-ratio range 1 and $\bar{\mu}$	13
6.5 Advance-ratio range 2 and $\bar{\mu}$	14
6.6 Advance-ratio range 3	15
6.7 General remarks on the advance-ratio ranges	15
6.8 Blade/vortex angle	16
7 APPLICATION	16
8 CONCLUSIONS	17
9 RECOMMENDATIONS	18
10 REFERENCES	18

CONTENTS (cont'd)

	page
APPENDICES	
A Number of blade sweeps over a point in the field behind the disc	19
B Intersection for particular ψ - and x -values	19
C Division of advance-ratio range 1	20
D Division of advance-ratio range 2	21
7 Tables	
8 Figures	

LIST OF SYMBOLS

Coordinate systems

X, Y Cartesian system; origin in blade tip at $\psi = 0$; X positive in direction of flight, Y (lateral axis) positive to starboard

ψ, x polar system; origin in rotor centre;

Unit values

R for distance (note particular definition of R)

ΩR for speed

B ratio between radius of vortex formation and tip radius

b number of blades per rotor

i index of arbitrary previous blade and tip vortex:
 $i=1$ immediately preceding blade
 $i=2$ pre-preceding blade
 $i=b$ tipvortex of the considered intersecting blade
 $i>b$ older part of tipvortex

j serial number, indicating rearward-concave parts of tip vortex (Fig. 1)

R radius of tip vortex formation

x radius of blade element, intersecting a tip vortex

η angle between blade and intersecting vortex (Fig. 2)

μ advance ratio between translational speed of rotor center in plane of disc and rotational tip speed ($x=1$)

ψ azimuth angle of blade, intersecting a tipvortex

ψ_t azimuth of blade with trailing vortex

Ω angular rotor speed

Indices

a	lowest	}	advance-ratio range in ranges 1 and 2
b	middle		
c	highest		
m	minimum value		

Superscripts

- advance-ratio range 1, including upper limit

= advance-ratio range 2, including upper limit

Abbreviations

AS advancing side of rotor disc, quadrants 1 and 2

FS front side of rotor disc, quadrant 2 and 3

Q quadrant of azimuth

RF reverse flow

RS retreating side of rotor disc, quadrants 3 and 4

1. INTRODUCTION

Near the tips of helicopter rotor blades, the bound circulation shows a steep gradient, leading to strong concentrated trailing vortices. Visualization by smoke or water vapor condensation has shown these vortices to remain close to the disc, in particular in forward flight. This has been confirmed by various theories on wake distortion. The combination of strong vortices and their proximity to the blades lead to large variations in induced velocity, blade angle of attack and aerodynamic loading. This is clearly evident from the results of numerous measurements of the chord- and spanwise pressure distributions on model and full-scale rotors: large peaks occur in the aerodynamic loading variation with azimuth, for various radial distances. Also several analytical methods exist, which have produced quantitative information on these effects.

The aerodynamic loading of rotor blades is of fundamental importance because it has a large influence with regard to:

- structural loads in blades, pitch horns and control rods
- fatigue
- vibration
- rotor aerodynamics, stall
- rotor stability and control
- rotor noise and blade slap.

The following study is mainly concerned with the geometry of helicopter rotor blade/vortex intersection in forward flight. This subject is simplified by assuming the vortices to remain undeformed in the plane of the disc. On this basis it can be proven that there are three successive main ranges of advance ratio, each with a different characteristic pattern of blade/vortex intersection. In addition, a subdivision is made of the lowest two ranges on the basis of secondary differences, resulting in a total of seven ranges, separated by six critical advance ratios.

In some publications on related problems, isolated results are shown on the blade position with respect to the vortices, but a more thorough and comprehensive study has not come to the attention of the author.

2. ASSUMPTIONS

The following analysis is based on a number of assumptions:

- vortex sheet rolled-up into concentrated tip vortex before intersection with blades
- tip vortices remain in the plane of the disc
- absence of in-plane tip vortex deformations
- radial distance of the point of tip vortex formation is constant
- line vortices (zero core radius)
- absence of root vortices
- equal blade spacing, due to:
 - . equal spacing of blade attachment points
 - . constant lag angle
 - . absence of lagwise bending.

Some of the simplifications just mentioned will further be elaborated on.

Behind a helicopter rotor blade, the *vortex sheet rolls up* into a concentrated tip vortex. According to flow measurements and visualization studies, this process is already well advanced at a short distance behind the blade. It is caused by the strong variation of bound circulation in spanwise direction. For helicopter rotors with a not too large number of blades, the roll-up has been completed before intersection occurs with a rotor blade.

Under normal operating conditions in forward flight at moderate to high μ , the tip vortices near the blades have just been formed and remain *close to the disc*. This is one of the reasons for the existence of aerodynamic loading peaks; these have been evidenced by many experiments (flow field measurements with speed sensors, smoke or tuft grid) and by theoretical analyses. The motion of a blade element over or under a tip vortex may then be approximated by an in-plane process and the term intersection may be used for simplicity. However, this assumption does not hold at low forward speed and near hovering flight conditions, wherein the induced velocity is large and the vortices are carried away in mainly downward direction.

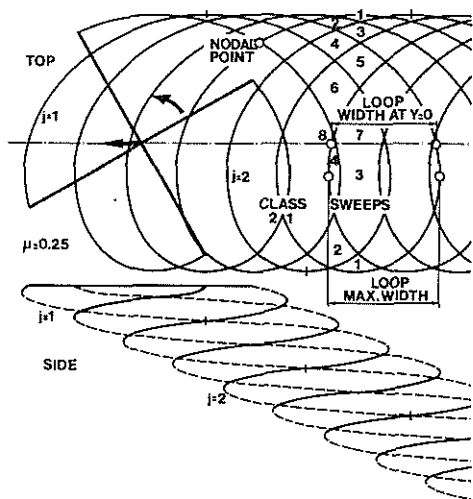


Fig. 1 Tip vortices in plan- and retreating-side view

The blade-tip path in forward flight closely resembles a trochoid. The assumption is that one may neglect the in-plane vortex *deformation*, which would occur due to the curvature of the vortex and the influence of bound and free vortices, in particular for those parts of the vortices close to the blades. This has been confirmed by various visualization experiments and by analysis. It is true that large distortions occur downstream of the disc, mainly near the port and starboard edges of the wake where

the vortices are close together. However, these deformations are mainly perpendicular to the disc and even there the in-plane deformations are still rather small.

The increase of the relative tangential airspeed towards the tip leads to a maximum bound circulation close to the tip and to a steep negative gradient and fall-off to zero at the tip. The radial position of the *point of tip-vortex formation* is therefore close to the tip and has been assumed to coincide with the tip: $x = 1$. The actual blade tip is then slightly more outward, at $x' = 1/B$.

The vortices considered are of the *line-vortex* type, with zero core radius. This assumption may be substantiated by noting that the vortices near the blades have only just been formed; so, their core size is small in comparison with that of older vortex parts. Furthermore, the position of the vortices will be considered in relation to the large disc; then, the small core diameter of only a few per cent of the rotor radius may be of little importance.

Vortices trailing from the more inward parts of the blade do not roll up into a clearly defined *root vortex* as counterpart of the tip vortex. It is therefore reasonable that theoretical analysis of rotors pay much more attention to tip vortices.

The blade attachment points are assumed to have equal *azimuthal spacing*, as for rotors of standard design. No attention is given to cases of irregular spacing in azimuth, as sometimes used for staggered or scissor tail rotors, or as investigated for main rotors of advanced design.

The lag angles of all blades are assumed to be constant. In combination with the foregoing assumption, this means that the blades and the

origins of their tip vortices remain equally spaced. It should be noted that the blade azimuth angle as used in this study refers to the actual blade position; in experimental investigations usually the hub azimuth position is used. The difference between these values is the constant component of the lag angle.

3. BLADE-ELEMENT PATH

3.1 Arbitrary blade element

The motion of blade elements consists of rotational and translational components with the dimensionless speeds x and μ . This motion is regarded as being due to rolling without slipping of a circle with radius μ in the plane of the disc over a base-line $Y = -\mu$ (Fig. 2). In polar coordinates:

$$x \sin \psi + \mu = 0 \quad (1)$$

This equation is used in section 6.3.1.

The momentary point of contact between the circle and base is given by ($\psi = 3\pi/2$; $x = \mu$); this is the point of the RF circle (radius $\mu/2$; equation $x = -\mu \sin \psi$) at the largest distance from the X-axis.

Each blade element describes a cycloid. The normal of this curve passes through the point of contact mentioned above; the centre of curvature is situated on that normal (but in general not in the point of contact). The distance, a blade element travels in X-direction during one complete rotation, is $2\pi\mu$.

Blade elements for which $x > \mu$ (such as is normally the case for the outer parts of helicopter blades, including the tip) describe cycloids with loops extending towards the retreating side of the base. Those elements for which $x \sin \psi + \mu = 0$ are temporarily located on the base; their direction of motion is only lateral. Elements at $x = \mu$ describe cycloids with a turning point on the base. Finally, the elements at $x < \mu$ remain on one side of the base, without describing loops. If $x = -\mu \sin \psi$ they are on the RF-circle and have no velocity in chord direction.

3.2 Tip element and tip vortex

The cycloidal shape of a tip vortex is determined by

$$X = \mu\psi_t - \cos \psi_t \quad (2)$$

$$Y = \sin \psi_t \quad (3)$$

Each trailing vortex can be divided into several parts, belonging to two classes, depending on whether the centres of curvature are situated towards the rear- or front side (Fig. 1). Parts of the first class, with their concave side facing rearward were generated by blades in the front side (FS) of the disc ($\pi/2 < \psi_t < 3\pi/2$: Q2 and Q3). If the rotor slipstream is seen as a skewed cylinder, these parts are on its front- or underside. Only vortex parts of this class make up the pattern of vortices in the disc and may intersect with the blades.

Vortex parts of the second class, with a forward facing concave side, were formed from blades in the aft side of the disc, in other words in Q4 and Q1. They are situated behind the disc and do not intersect with blades in the disc.

- For arbitrary μ , there are several particular points of a tip vortex.
- $Y = 0$, $\psi' = 0$ and π . The slope dY/dX of the vortex can be determined from Eqs. (2) and (3) and this results in $\pm 1/\mu$.
 - The lateral distance Y of the nodal points of a tip vortex from the X-axis (centre line) can be determined from the following equation, given without derivation:

$$\cos \psi' = \mu(\pi/2 + \psi') \quad (4)$$

with

$$Y = \sin \psi' \quad (5)$$

- The maximum width of a vortex loop, measured in longitudinal direction at $Y = -\mu$, follows from

$$\text{width} = (2 \arcsin \mu - \pi) \mu + 2(1 - \mu^2)^{\frac{1}{2}} \quad (6)$$

The width decreases for increasing values of μ .

- The width of the loop measured along the X-axis is less than the maximum width as determined under c). The difference (given without derivation) is:

$$2[\mu \arcsin \mu + (1 - \mu^2)^{\frac{1}{2}} - 1] \quad (7)$$

This result is used in section 6.4 for the determination of the first main critical advance ratio $\bar{\mu}$.

Two particular values of μ that are independent of the number of blades per rotor can be derived as follows.

- The width of the loop measured along the X-axis is equal to 1. Using the result of d) above, one finds $\mu = 1/\pi = 0.318$. This result, which lies in the practical range for helicopters, is of importance for determining the number of blade sweeps over a given point on the RS.
- The nodal point mentioned under b) is situated on the X-axis for $\mu = 2/\pi = 0.637$, which is twice the value calculated under e). It is well beyond the normal range of advance ratios for helicopters.

There are also specific μ -values which are dependent on the number of blades. These are in fact the subject of this report. One of these μ -values has been mentioned under d). Section 6.4 contains the complete information.

With respect to the aerodynamics of a single tip vortex, the following statements are useful. It is noted that the induced downflow occurs on the concave side and upflow on the convex side. So, the vortex parts of the first class, present in the rotor disc, induce downflow behind the vortex, whereas parts of the second class induce downflow on their forward facing side. The flow field around the cycloidal vortex, however, is very complex because of its varying circulation and curvature. For a simple approximation one could replace the cycloid by a circular vortex with the same radius of curvature as the cycloid has near the point of interest. Theoretical results for a single circular vortex are known from literature. These show that the induced velocity at a point increases due to vortex curvature towards that point.

4. TIP-VORTEX PATTERN OF A ROTOR

Figure 1 shows the schematic pattern of the free vortices as projected on the plane of the disc.

The longitudinal spacing between successive vortices is $2\pi\mu/b$, this being the ratio of the distance travelled by the rotor during one revolution and the number of tip vortices formed. This spacing is independent of the lateral coordinate Y . From photographs of rotors with external or blade-tip smoke sources, it can be established that the actual vortex spacing is in good agreement with this expression. It means that vortex deformations parallel to the disc are small, in particular near the disc. This is obviously of importance for a simple determination of the blade/vortex intersection.

There are some notable differences between the vortex patterns within and behind (but in the plane of) the disc. The former case is characterized by the presence of only rearward concave vortices, without mutual intersection. Their number is about $b/(\pi\mu)$.

The area behind the disc is covered by mutually crossing vortex parts. More details are contained in Appendix A. This also deals with the number of blade sweeps over a point in the field behind the disc.

5. BLADE/TIP-VORTEX INTERSECTION

5.1 Main parameters

The influence of a free vortex on the aerodynamic loading of a blade element is mainly determined by:

- a) rotor operating condition (tip speed and advance ratio)
 - b) radius x of blade element
 - c) tip-vortex strength
 - d) vertical distance between blade and vortex (assumed zero in this paper).
- The parameters under a) and b) determine the azimuth of intersection for the blade element and the relative position of blade and vortex. These aspects are dealt with in the following sections.

5.2 Derivation of intersection formula

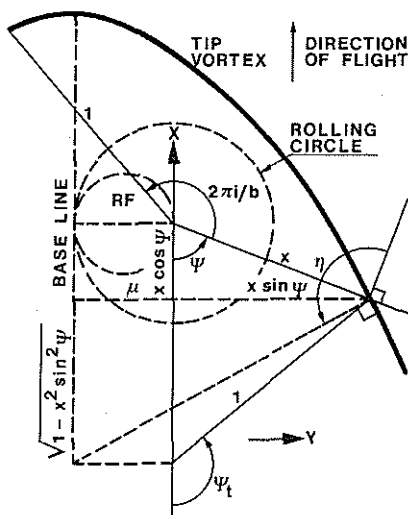


Fig. 2 Derivation of formulae for intersection and angle η between blade and vortex

Figure 2 shows a blade at azimuth ψ and its element at radius x intersecting the tip vortex of a previous blade. Two rotor positions are considered, viz. the forward position where intersection occurs, and a rearward position where the intersecting part of the tip vortex was formed. The distance between both rotor centres is $x \cos \psi + (1 - x^2 \sin^2 \psi)^{1/2}$.

This distance is by definition equal to μ times the difference in azimuth angles between the two positions considered. Now, the azimuth at the moment of intersection is $\psi + 2\pi/b$. However, the part of the tip vortex was generated when the i -th preceding blade was at azimuth $\arcsin(x \sin \psi)$. Care should be exercised with this multi-valued

function. Preference is therefore given to the principal value only. Then the azimuth must be expressed as $\pi - \arcsin(x \sin \psi)$ to obtain the value for the first ($j = 1$) tip-vortex part (Section 3.2) on the FS of the disc (Ch. 4). To deal also with earlier produced parts with numbers $j > 1$, the expression is extended to $\pi - \arcsin(x \sin \psi) - (j - 1)2\pi$. Then, the angular difference mentioned above becomes $\psi - [3 - 2(j + i/b)] \pi + \arcsin(x \sin \psi)$. It is seen that increasing j by 1 to obtain the next rearward-concave vortex part is equivalent to an increase of i by b , both operations increasing the value of the expression by 2π . This effect can also be obtained by increasing ψ by this amount. For simplicity, j may be put equal to 1 and the expression is $\psi - (1 - 2i/b)\pi + \arcsin(x \sin \psi)$, in which i may be larger than b for higher vortex part numbers.

The final equation for determining intersection conditions now becomes

$$x \cos \psi + (1 - x^2 \sin^2 \psi)^{\frac{1}{2}} - [\psi - (1 - \frac{2}{b/i})\pi + \arcsin(x \sin \psi)] \mu = 0 \quad (8)$$

This is the basic expression from which many other formulae in this report are derived.

The coordinates ψ and x of the points of intersection, in the polar system translating with the rotor, depend only on b/i and μ .

In order to obtain all intersections (for all tip vortices and all vortex parts), the blade-or vortex index should be chosen $i = 1, 2, 3$, etc. The final value is reached when during one complete revolution the blade does no longer show any intersections.

5.3 Particular ψ - and x -values

For several particular values of ψ and x , equation (8) reduces to simpler forms (Appendix B). These cases give some additional insight into the pattern of lines for constant μ in the polar plots. However, no aerodynamic importance should be attached to these cases.

5.4 Blade/vortex angle

Based on the definition of the angle η between blade and intersecting vortex (Fig. 2) and on the fact that such a vortex is concave towards the rear, it is possible to make some general remarks, as indicated in the scheme below.

Blade/vortex intersection	Angle η position	$-\pi/2$ perp.	0 tangent	$\pi/2$ perp.	$\pm \pi$ tangent
	Concave side towards	tip	leading edge	rotor centre	trailing edge
possible in quadrants	1, 4 aft	4, 3 RS	3, 2 FS	2, 1 AS	

A formula for η can be derived from Figure 2, which results in:

$$\eta = \pi - \psi + \arctan [(1 - x^2 \sin^2 \psi)^{\frac{1}{2}} / (\mu + x \sin \psi)] \quad (9)$$

Herein, combinations of $(\psi; x; \mu)$ must be substituted which satisfy Eq. (8). The multi-valued function \arctan is chosen such that $-\pi \leq \eta \leq \pi$.

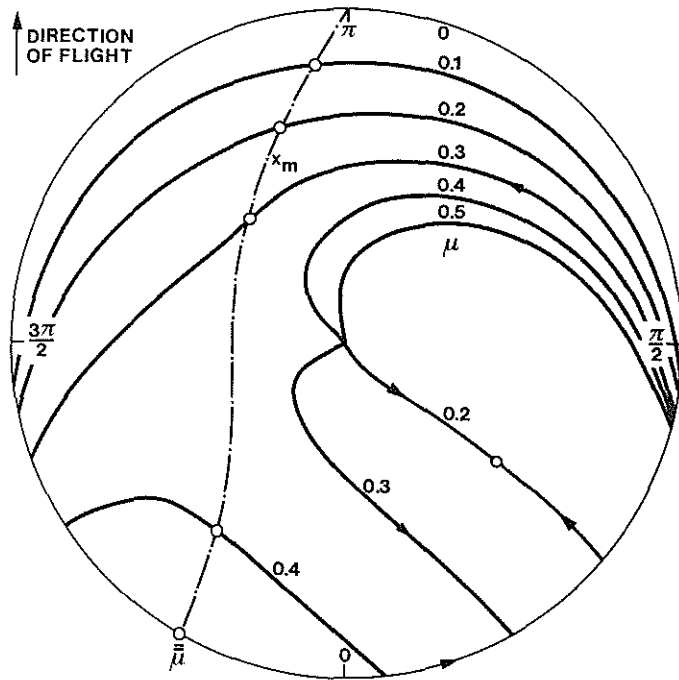


Fig. 3 Example of intersection pattern
 $\mu = 0 (0.1) 0.5$; $b/i = 4$

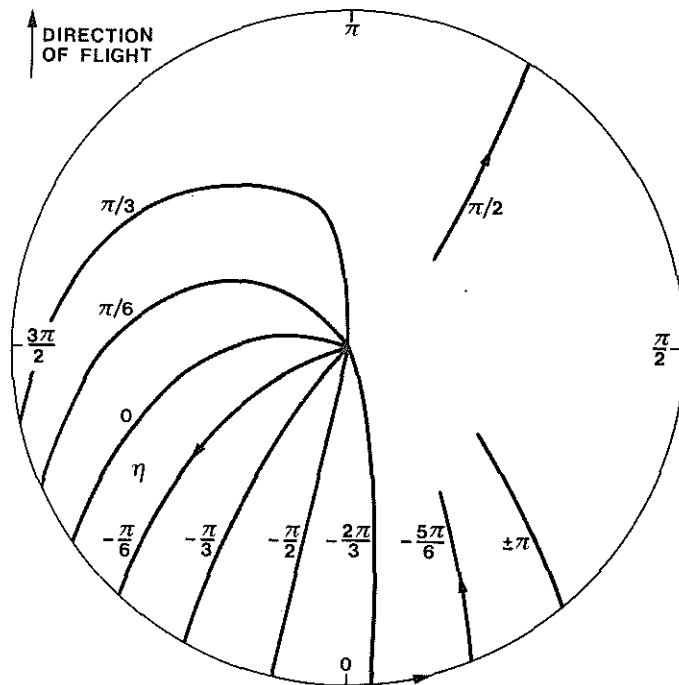


Fig. 4 Example of blade/vortex angle pattern
 $\eta = 0 (\pm\pi/6) \pm\pi$; $b/i = 4$

It follows that η depends on $(\psi; x)$ and μ ; because of Eq. (8), also b/i is involved.

5.5 Numerical results

Results for the intersection and the angle η can be calculated for fixed values of b/i and μ and plotted in polar diagrams.

Each point of an intersection curve gives the combination $(\psi; x)$ where intersection occurs with the i -th preceding vortex. An example is shown in figure 3 for $b/i = 4$, with intersection lines for constant μ at intervals of 0.1. This applies to a four-bladed rotor and the intersection with the immediately preceding blade vortex (or to an eight-bladed rotor and the pre-preceding vortex, etc.).

The full range of parameters for which intersection plots have been made is determined by $0 \leq \mu \leq 0.6$; $i = 1, 2$ and b , and $1 \leq b \leq 7$.

The corresponding results for the intersection angle η at intervals of $\pi/6$ have been plotted in figure 4. The general trend for the entire range of b/i -values is identical; therefore only one specific value of b/i is used to represent the results.

6. DISCUSSION

6.1 Common characteristics of intersection

Between the various intersection patterns for the combinations of b/i and μ , a number of commonalities exist. These are evident in figures 3 and 5 and in the figures in tables 2, 3 and 4 which are fully discussed later.

- a) There is no crossing of lines for different μ -values, except at the rotor centre; each point of the disc belongs to a unique μ -value at which intersection occurs.
- b) The μ -lines do not exhibit branching points, except the line for the first main critical advance ratio $\bar{\mu}$ (Section 6.4) at $(\psi = 3\pi/2; x = \bar{\mu})$.
- c) Before the blade tip reaches the intersecting vortex, it rotates through an azimuth interval in Q1 without intersections.
- d) The advancing tip intersects the preceding vortex in Q1, just before $\psi = \pi/2$, from where the point of intersection starts to move inward along the blade (branch 1).
- e) The rotor centre intersects the vortex for each value of μ . It depends on the μ -ranges to be discussed whether the intersection point starts to move outward along the blade or leaves the blade at that point. The region of the blade from the centre outward to x_m (Section 6.3.1) is called the inner region. All elements in this region intersect the preceding vortex once.

6.2 Main advance-ratio ranges

An inspection of the intersection patterns for various advance ratios shows the existence of three main ranges (Fig. 5), differing fundamentally with respect to:

- variation of the radius of intersection over the blade span
 - existence of x_m and its variation with μ
 - number of intersections per revolution
 - maximum number of sweeps over field point in the plane behind the disc
- These ranges are called range 1, 2 and 3; they are separated by the first and second main critical advance ratios $\bar{\mu}$ and $\bar{\bar{\mu}}$, respectively. Their characteristics are indicated in Table 1 and 2. In range 1 ($0 < \mu < \bar{\mu}$) the

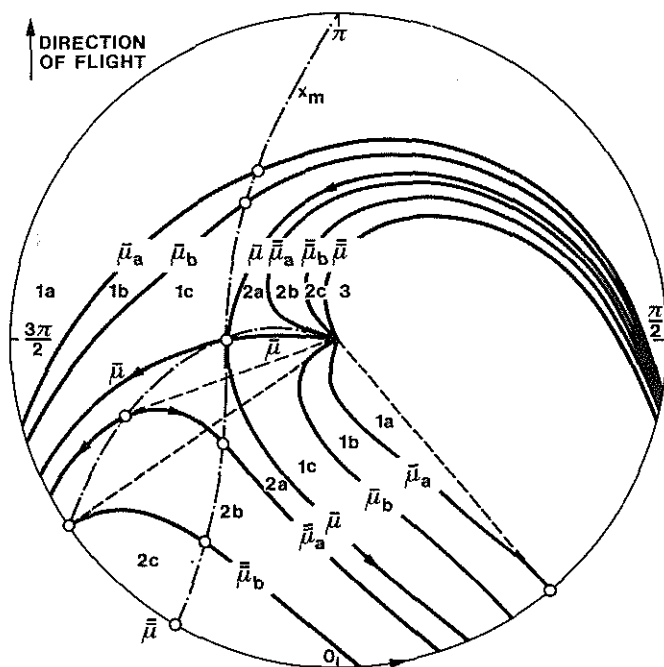


Fig. 5 Intersection patterns for critical advance ratios and situation of advance-ratio ranges; $b/i = 4$

intersection point of Q1 moves inward over branch 1 through the outer region until x_m , then outward and leaves the blade at the tip in Q3. For range 2 ($\bar{\mu} < \mu < \bar{\bar{\mu}}$) the intersection point moves inward along branch 1 over the whole blade span and leaves the blade at the rotor centre; a second intersection branch runs through Q4 and Q1, and this now determines the separation between the inner- and outer blade region. In range 3 ($\bar{\bar{\mu}} < \mu$) there is only branch 1, starting at the tip in Q1 and leaving the blade at the rotor centre.

Ranges 1 and 2 may each be subdivided in 3 subranges a, b and c, according to less fundamental differences. These are indicated in Table 3 and 4 and discussed in Appendices C and D. A complete survey of the main- and sub-ranges is shown in figure 5.

6.3 Common characteristics of μ -ranges 1 and 2

For the intersection curves in the μ -range covered by the combination of ranges 1 and 2, there are 3 kinds of particular situations. It is therefore useful to deal with them before discussing the separate ranges.

6.3.1 Minimum radius

In the ranges 1 and 2 there is for each ($b/i; \mu$) combination a minimum radius x_m . The blade elements beyond x_m , in the outer blade region, make two more intersections per revolution than those of the inner region (Tables 3 and 4).

The value x_m is found from the condition $dx/d\psi = 0$ for constant μ . Determining this derivative from Eq. (8) results in the equation $x_m \sin \psi_m + \mu = 0$. This is Eq. (1) of the base of the trochoids. It is seen that $\sin \psi_m \leq 0$, which indicates that x_m will occur in Q3 and/or Q4. Because the x_m -element is momentarily on the base, it will then move laterally while touching the tip vortex.

The minimum radius may be determined from the combination of Eqs. (1) and (8). The simplest way is to eliminate first x_m . This yields

$$\psi_m + \cotan \psi_m - \left(1 - \frac{2}{b/i}\right)\pi = \arcsin \mu + (1 - \mu^2)^{1/2}/\mu, \quad (10)$$

from which ψ_m may be determined. Finally x_m follows from Eq. (1). The resulting variation of x_m with μ is shown schematically in figures 3 and 5. The x_m -line starts at $(\pi; 1)$ for $\mu = 0$, in which case the whole blade lies in the inner region. The x_m -line in Q3 belongs to μ -range 1 and continues to $(3\pi/2; \bar{\mu})$. At this point the inner region extends towards $x_m = \bar{\mu}$; this is the minimum value of x_m . The part of the x_m -line in Q4 applies to

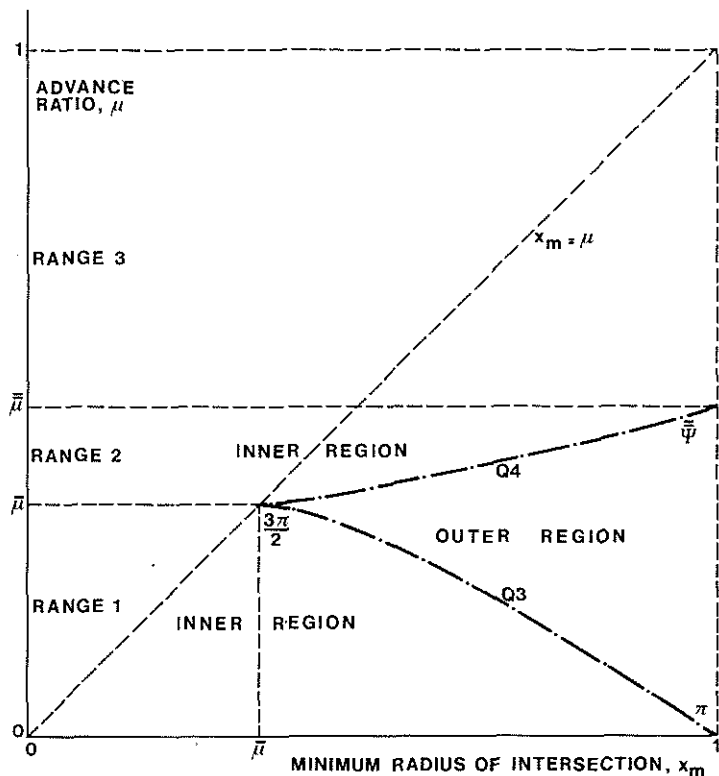


Fig. 6 Variation of minimum radius of intersection x_m with advance ratio; $b/i = 4$

6.3.2 Tip intersection on rear side

In addition to the tip intersection in Q1, as discussed in the third part of Appendix B, there are two more blade tip intersections in Q4 and 1 for μ -ranges 1 and 2 (never in Q2 and 3). Eq. (B4) for calculating the azimuth as a function of μ is given in Appendix B, but the factor of π should now be $-(1.5 - \frac{1}{b/i})$ for Q4 and $+(0.5 + \frac{1}{b/i})$ for Q1 because older parts of vortex i must be considered.

Some numerical results are shown in figure 3. For range 1, the two roots for $x = 1$ represent the outer points for two different branches of the intersection curve. The azimuth of the end-point of branch 1 is only slightly larger than $3\pi/2$. In the case of range 2, the two roots are the outer points of branch 2. Whether the intersection point with the smallest ψ leaves the blade at the tip or starts its way along the blade is discussed in Appendices C and D. As μ is increased, the ψ -values of these tip intersection points approach each other, becoming $\bar{\psi}$ in Q4 as $\bar{\mu}$ is reached.

6.3.3 Radial tangent

There are certain μ -ranges in which the blade becomes tangent to a preceding vortex at some azimuth. The aerodynamic influence of the vortex will then extend over a considerable radial length of the blade. Also, when slightly changing the azimuth around that position, the number of intersections of a blade with the vortex will change by 2. Finally it may be anticipated that the rate of change of x with azimuth will be large. With respect to the intersection line for constant μ , this means that it will also have a radial tangent. The three cases of this tangent situation may be seen in the figures:

μ -range 2. The inner region grows with increasing μ and finally $x_m = 1$ at $\bar{\psi}$, where the outer region has disappeared from the blade (beginning of range 3).

The picture presented above may also be demonstrated by using figure 6, which gives the variation of x_m with μ for constant b/i . For combinations of x_m and μ , the azimuth ψ_m may again be calculated from Eq. (1).

Table 3, left, branch 2 near tip in Q1	Table 4, left branch 1 near rotor centre in Q3	Table 4, left and middle branch 2 near tip in Q4
--	--	--

The analysis of these cases may start from Eq. (8) by using the condition $d\psi/dx = 0$ for constant μ , or from Eq. (9) with $\eta = 0$ or π . Both derivations lead to

$$\mu = -x \sin \psi + (1 - x^2 \sin^2 \psi)^{\frac{1}{2}} \cotan \psi . \quad (11)$$

Combining this with Eq. (8) enables the elimination of μ and the determination of the coordinates (ψ ; x) of the intersection points having a radial tangent.

If these points are situated at $x = 1$ or 0 , the corresponding μ is critical, because exceeding these values leads to a change in the number of simultaneous intersection points on a blade. These critical ratios are $\bar{\mu}_a$ (radial tangent at $x = 1$ in Q1), $\bar{\mu}_B$ (radial tangent at $x = 0$ in Q3) and $\bar{\mu}_b$ (radial tangent at $x = 1$ in Q4). Their details are discussed in appendices C and D. The ranges referred to in the beginning of this section are numbered 1a, 2a and 2b.

6.4 Advance-ratio range 1 and $\bar{\mu}$

The limits of range 1 are given by $0 < \mu < \bar{\mu}$; the intersection pattern consists of 2 branches (Table 3).

Branch 1 starts in Q1 at the tip, from where the intersection point moves inward. The minimum x occurs in Q3 at $\psi = \pi + \arcsin \mu/x_m$, so that the inward motion is completed over an azimuth interval greater than $\pi/2$. Thereafter x increases and the intersection point leaves the blade in Q4. The inner elements $0 < x < x_m$ do not intersect on this branch, but for the outer elements $x_m < x < 1$ two intersections occur. With increasing μ , the minimum radius x_m decreases from 1 at $\psi = \pi$ for $\mu = 0$ to $x_m = \bar{\mu}$ at $\psi = 3\pi/2$ for $\mu = \bar{\mu}$.

Branch 2 of intersection points for an older part of the same vortex starts at $x = 0$ for ψ in Q3 or Q4 and extends over the region $0 \leq x \leq 1$. This leads to an additional intersection of each blade element per revolution. Therefore, in total the inner elements meet the vortex only once, whereas the outer elements intersect three times per revolution.

Details on the division of advance-ratio range 1 into 3 subranges with separating advance ratios $\bar{\mu}_a$ and $\bar{\mu}_b$ are presented in Appendix C and Table 3. Numerical results are shown in Table 6, as well as in figures 5 and 7.

At the upper limit of ranges 1 or 1c, the intersection pattern of range 1 (with branch 1 from $x = 1$ over x_m to 1) changes into the pattern for range 2. This occurs at the first main critical advance ratio $\bar{\mu}$, when intersection branches 1 and 2 meet at $(3\pi/2; \bar{\mu} = x_m)$. See table 2, left, for a description and figure 5. Because of these intersection coordinates, the blade is then tangent to the preceding vortex at $\psi = 3\pi/2; x = \bar{\mu}$.

The formula for determining the first main critical advance ratio $\bar{\mu}$ follows from Eq. (8) by putting $\psi = 3\pi/2$ and $x = \bar{\mu}$:

$$(1 - \bar{\mu}^2)^{\frac{1}{2}} - [(\frac{1}{2} + \frac{2}{b/i})\pi - \arcsin \bar{\mu}] \bar{\mu} = 0 . \quad (12)$$

Another derivation of this equation uses Eq. (7), setting $(1 + \text{width difference}/2)$ equal to the product of μ and the rotation angle $(\frac{1}{2} + \frac{2}{b/i})\pi$.

By using a new parameter $\bar{\psi}$ in Q4, defined by

$$\bar{\mu} = -\sin \bar{\psi} \quad , \quad (13)$$

Eq. (12) can be somewhat simplified to

$$\bar{\psi} + \cotan \bar{\psi} = \left(\frac{3}{2} - \frac{2}{b/i}\right)\pi \quad . \quad (14)$$

Numerical results are shown in Table 6 and 7 and figure 7. These follow the general trend of all critical advance ratios, namely increasing with b/i .

The first main critical advance ratio is not only important because it determines the boundary between two different characteristic patterns of the intersection lines. It has a similar role with respect to the maximum number of blade sweeps over a point in the flow field behind the disc. This is explained in Appendix A; the result is shown in Table 1, bottom line.

6.5 Advance-ratio range 2 and $\bar{\mu}$

The limits of range 2 are given by $\bar{\mu} < \mu < \bar{\bar{\mu}}$; again the intersection pattern consists of two branches (Table 4).

Branch 1 starts in Q1 at the tip, from where the intersection point moves inward until the rotor centre is reached at an azimuth determined by Eq. (B5).

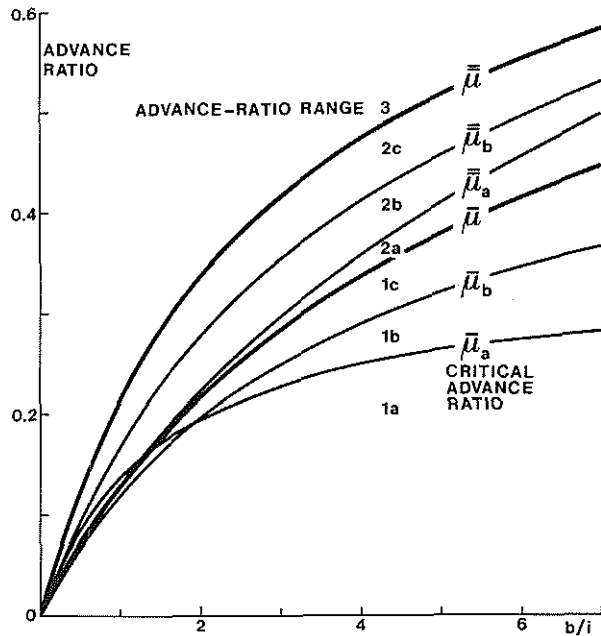


Fig. 7 Advance-ratio ranges and critical advance ratios as a function of the ratio b/i between the number of blades per rotor b and the index i of a preceding blade

If μ increases, the extent of the inner blade region becomes larger and the intersection branch 2 shrinks until the two points at $x = 1$ coincide in Q4. Then $x_m = 1$: the outer region has vanished. The blade tip touches the preceding vortex with number i and this implies that all vortex loops

Branch 2 of intersection points with an older part of the same vortex is located in Q4 and Q1, or Q4 only, and contains the intersections of the blade elements of the outer region, with x_m occurring in Q4 at $\psi_m = 2\pi - \arcsin \mu/x_m$.

This pattern results in the same number of intersections per revolution for the inner and outer regions as in μ -range 1, namely 1 and 3 respectively.

Between the azimuth intervals having intersections with branches 1 and 2, there are always two intervals without intersections.

Details on the division of advance-ratio range 2 into 3 subranges with their separating advance ratios $\bar{\mu}_a$ and $\bar{\mu}_b$ are presented in Appendix D and Table 4. Numerical results are shown in Table 6, as well as in figures 5 and 7.

behind the disc are tangent to each other (at $Y = -\bar{\mu}$). A description of the intersection pattern is contained in Table 2, wherein it is also possible to compare the characteristics with those for $\bar{\mu}$.

The second main critical advance ratio $\bar{\bar{\mu}}$ follows from Eqs. (10) and (1) with $x = 1$:

$$(1 - \bar{\mu}^2)^{\frac{1}{2}} - [(\frac{1}{2} + \frac{1}{b/i})\pi - \arcsin \bar{\mu}] \bar{\mu} = 0 . \quad (15)$$

By using a new parameter $\bar{\psi}$ in $Q4$, defined by

$$\bar{\mu} = - \sin \bar{\psi} , \quad (16)$$

this can be written as

$$\bar{\psi} + \cotan \bar{\psi} = (\frac{3}{2} - \frac{1}{b/i})\pi . \quad (17)$$

Numerical results are shown in Tables 6 and 7 and figure 7. This $\bar{\bar{\mu}}$ is the highest of the 6 critical ratios discussed. Above $\bar{\bar{\mu}}$ there are no more characteristic changes in the intersection pattern.

This second main critical advance ratio $\bar{\bar{\mu}}$, just like $\bar{\mu}$, determines also a characteristic change in the maximum number of blade sweeps over a point in the field behind the disc (Appendix A and Table 1, bottom line).

A comparison of Eq. (15) with Eq. (12) for $\bar{\mu}$ shows, that these only differ in the denominator of the term with b/i . This leads to the simple relation

$$\bar{\mu}_{2b/i} = \bar{\bar{\mu}}_{b/i} . \quad (18)$$

This is also shown in Tables 6 and 7. In physical terms it means that a rotor at the first main critical advance ratio $\bar{\mu}$ with respect to the preceding vortex i (blade at $\psi = 3\pi/2$ and $x = \bar{\mu}$ tangent to vortex) is also operating at the second main critical advance ratio $\bar{\bar{\mu}}$ with respect to the vortex with index $2i$ (blade tip moves laterally along vortex $2i$ in $Q4$). See also the text in Table 2. However, if a rotor is operating at $\bar{\mu}$ for an odd index i , then the $\bar{\bar{\mu}}$ -situation does not occur simultaneously.

6.6 Advance ratio range 3

For $\mu > \bar{\bar{\mu}}$ the inner region covers the whole blade and the intersection pattern consists only of branch 1. Its description is contained in Table 5. The general Eq. (8) must be used for the calculation of the points of intersection.

6.7 General remarks on the advance-ratio ranges

The μ -range in which a rotor is operating depends on the number of blades and on the index of the preceding vortex considered. To explain this more fully, Table 7 shows the two main critical advance ratios as functions of the separated variables b and i . As an example it may be noted that a three-bladed rotor at $\mu = 0.2$ is in range 1 if the immediately preceding tip vortex is considered ($i = 1$); however, for $i = 2$ and 3 the range 2 and for $i = 4$ the range 3 is applicable. Similar comparisons could be made with the other critical advance ratios $\bar{\mu}_a$, $\bar{\mu}_b$, $\bar{\bar{\mu}}_a$ and $\bar{\bar{\mu}}_b$.

However, as the immediately preceding vortex has generally the largest aerodynamic influence, it is proposed to indicate the rotor operating

condition by the name of the advance-ratio range based on this vortex ($i = 1$).

The fact that the total μ -range may theoretically be divided into ranges with different intersection patterns makes it probable that the corresponding changes in patterns may be recognized in the variation of some rotor quantities with μ . The "ripple" as noted by HILL in experimental data of power required in level flight for several helicopter types may be such a case (Ref. 1). See Ch. 7 and figure 8.

The absence of similar characteristic changes for fixed-wing aircraft may too long have led to the belief in perfectly smooth curves for the variation of helicopter rotor characteristics with μ . It has now theoretically been clarified that a chance exists for kinks or ripples.

6.8 Blade/vortex angle

In figure 4 and similar figures for other values of b/i , the following can be noted with regard to the angle η between the blade and the vortex at the moment of intersection. The parameter b/i has little effect on the total character of the plots such as figure 4 and some general remarks can be made.

Where the blade tip first comes close to the vortex, in Q1, η is about 120 to 140°, and decreases to about 90° (vortex perpendicular to blade with concave side towards rotor centre) as the blade rotates in Q2. There is a large area here around $\eta = 90^\circ$ with only small variations both with ψ and x . When the RS is approached, the angle further decreases until $\eta = 0$. The intersection angle for rearward-pointing blades is about -90 to -120°. Finally, η becomes $\pm 180^\circ$ in Q1. In total the area for positive η is considerably larger than for negative values.

All lines for constant η pass through the rotor centre because η is indefinite at that point.

Two particular cases can be distinguished.

- a) $\eta = 0$ and $\pm\pi$. The blade is tangent to the vortex. For a slightly larger azimuth, the blade will start to be intersected at two closely spaced points, respectively the blade has just moved towards the convex vortex side and the originally two closely spaced intersection points have coincided and moved off the blade. For both cases the intersection line for constant μ has a radial tangent. According to this property, the lines for $\eta = 0$ and $\pm\pi$ in figure 4 are identical with the dotted lines for the radial tangent in figure 5.
- b) According to section 6.3.1, a particular meaning can be attached to those points of the intersection lines for constant μ which are situated on the base $Y = -\mu$ of the trochoids. These points are namely located on the line for which the minimum value x_m of x occurs. This passes through the points with polar coordinates $(\pi; \bar{1})$, $(3\pi/2; \bar{\mu})$ and $(\bar{\psi}; 1)$. Combination of Eq. (1) for the base and Eq. (9) for η results in the following equation for η on the x_m line:

$$\eta = 3\pi/2 - \psi . \quad (19)$$

7. APPLICATION

In reference 1, A.B. Hill of the US Naval Air Test Center noted a "ripple" in experimental data of power required for the main rotor in level flight, for several helicopter types. This ripple represents a slight but important power increase at airspeeds slightly above the speed for minimum power. The mean total width of the ripples is about $\Delta\mu = 0.045$. The ripple

location is independent of the rotor thrust coefficient. In the power required curve of a tandem rotor helicopter, two consecutive ripples are noteworthy. The author has observed mixed reactions to this ripple concept during discussions with flight test engineers and data analysts.

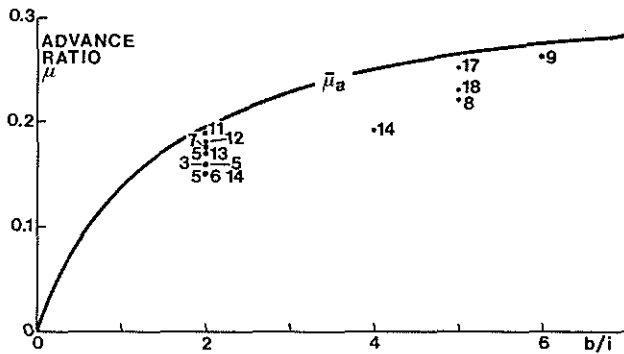


Fig. 8 Comparison between critical advance ratio $\bar{\mu}_a$ with experimental points for the position of a ripple in the powered required curve for level flight for several helicopters. Reference 1 data plotted for preceding vortex index $i = 1$ with orig. fig. nbr.

to exist between μ -values for the ripples and $\bar{\mu}_a$. Then, one may cautiously conclude that the corresponding blade/vortex intersection pattern may be responsible for the increase in power required at that advance ratio.

The mean advance ratios of the ripples have been plotted in figure 8 on b/i , using $i = 1$. The numbers at the data points refer to the figures of reference 1.

These experimental results are now compared with those of the present analysis. For this purpose, figure 8 also shows the theoretical line for $\bar{\mu}_a$, the lowest of the critical advance ratios. At this $\bar{\mu}_a$ the blade is tangent at the tip to the preceding tip vortex, in Q1. This situation may lead to an increase in the relative tangential airspeed and angle of attack over a considerable blade region from the tip inwards. From figure 8, a remarkable correlation appears

8. CONCLUSIONS

A theoretical study on the geometry of blade/vortex intersection in the plane of the disc has led to an insight in the various intersection characteristics and to the corresponding quantitative results. These pertain to a single rotor with b blades and intersection with the i -th preceding tip vortex. The results of the analysis may be used to improve the understanding of the variation of experimental and theoretical data on blade loading with azimuth and on rotor characteristics with advance ratio. The main conclusions are as follows.

1. Seven ranges of advance ratio can be distinguished, each with specific characteristics with regard to intersection pattern, number of intersections per revolution and number of simultaneous intersections on the blade.
2. Also in the flow field behind the disc, characteristic differences are noticeable in these ranges, namely in the location of the vortices and the maximum number of blade sweeps over a point in the flow field.
3. These ranges are bounded by six critical advance ratios $\bar{\mu}_a$, $\bar{\mu}_b$, $\bar{\mu}$, $\bar{\mu}_a$, $\bar{\mu}_b$, and $\bar{\mu}$, which only depend on the ratio b/i between the number of rotor blades b and the index i of the preceding vortex. These critical advance ratios increase and are mutually further apart when b/i increases. For a rotor with a given number of blades and operating at a certain advance ratio, the advance-ratio range depends on the index of the preceding tip vortex.
4. The third and sixth are the main critical advance ratios $\bar{\mu}$, and $\bar{\mu}$, at which the characteristics considered show principal changes.
5. If a rotor operates at $\bar{\mu}$ based on the i -th preceding tip vortex, it is

also operating at $\bar{\mu}$ based on the $2i$ -th preceding tip vortex. However, if a rotor is operating at $\bar{\mu}$ based on an odd tip vortex index i , then the intersection pattern is only critical in this respect and not with regard to $\bar{\mu}$.

6. The 4th-critical advance ratio $\bar{\mu}_a$ has probably no practical significance.
7. The existence of critical advance ratios might lead to ripples or kinks in the variation of several rotor characteristics with advance ratio.
8. The theoretical trend of the first critical advance ratio $\bar{\mu}_a$ as a function of b/i correlates with the experimental data collected by HILL on the position of a ripple in the curve for power required in level flight for several helicopter types. This correlation is based on the assumption that the immediately preceding tip vortex is the one most involved ($i = 1$). The required-power increase may be due to the blade being tangent to the tip vortex in the first quadrant. This may well lead to an increased tangential airspeed and angle of attack over a large region of the blade from the tip inward.

9. RECOMMENDATIONS

It is recommended to continue this theoretical study by translating the insight obtained in the geometry of blade/vortex intersection into its aerodynamic consequences. In particular, standard azimuthal variations of aerodynamic blade loading could be determined for the various advance-ratio ranges (and critical advance ratios) and for the inner and outer blade regions. This may lead to a set of qualitative plots, to which experimental data can be compared. Moreover, it seems useful to investigate in the same manner the variation of the blade torsional moment, in particular in the various situations wherein the blade is tangent to the vortex.

Another extension of this theory might be towards coaxial and tandem rotors, although the assumption of an in-plane process is then becoming more questionable.

Finally, it seems advisable to reconsider the methods used for calculating the rotor power required in forward flight. Especially it should be verified whether these are suitable to account for a required-power increase, due to a blade becoming tangent at the tip to the immediately preceding tip vortex in the first azimuth quadrant. It could also be useful to reconsider earlier results of calculations and measurements, in particular those cases where ripples have been removed by unjustified data smoothing.

10. REFERENCES

- 1) A.B. Hill, A new look at helicopter level flight performance. AGARD-CP-121 on Advanced Rotorcraft Vol I, paper 6 (1971)

Acknowledgement

The calculations required for this investigation have been performed by Mr. M.A.P.J. Horsthuis, whose dedicated assistance is gratefully acknowledged.

APPENDIX A

Number of blade sweeps over a point in the field behind the disc

Behind the disc, the vortices are concave, either downstream or upstream (Fig. 1). The first class is a continuation of the vortices in the disc and the other class contains those on the upper side of the slipstream.

Each point of the field behind the disc has experienced its final *number of blade sweeps*. The following rules can be given for determining this number.

On the advancing side the number of sweeps is constant in each polygon formed by intersecting tip vortices. By passing over a vortex to a neighbouring polygon, the number of sweeps is changed by 1 (if going from the convex to the concave side: +1, otherwise -1). The triangular polygon near the vertex, along the starboard side of the disc, experiences only one sweep. The maximum number occurs in AS-polygons bordering the X-axis; this number depends on the applicable μ -range as discussed in Ch. 6.2. The results are indicated in Table 1, bottom line.

The rules for the number of sweeps on the RS are less simple. However, leaving aside some exceptions, it can be stated that the number of blade sweeps in RS-polygons is less than on the AS. The difference in numbers between neighbouring polygons along the X-axis is often equal to b . The minimum value within a polygon is 1 and this occurs near the vertex of each vortex loop. For high μ there are large areas wherein the points of the field do not experience any blade passage at all.

For the induced velocity, not only the number of sweeps is important, but also the aerodynamic loading on the blade as it passes a field point. This effect is not the subject of this paper.

APPENDIX B

Intersection for particular ψ - and x -values

Forward-pointing blade.

The introduction of $\psi = \pi$ in Eq. (8) leads to

$$x = 1 - 2\pi\mu/(b/i) \quad . \quad (B1)$$

This is a linear relationship between x and μ , so that the curves for equidistant values of μ divide the X-axis into equal parts (Fig. 3). The proportionality factor is $-2\pi/(b/i)$. The blade is therefore intersected closer to the hub for higher advance ratios. Beyond $\mu = b/(2\pi i)$ there are no more intersections (at positive radial distances x).

Rearward-pointing blade

For azimuth $\psi = 2\pi$, Eq. (8) becomes

$$x = \left(1 + \frac{2}{b/i}\right)\pi\mu - 1 \quad . \quad (B2)$$

This is again linear, (Fig. 3), but now the proportionality factor is positive and larger in absolute sense than for $\psi = \pi$. The points of intersection move towards the tip as μ becomes larger. There are no more intersections on the blade beyond

$$\mu = \frac{2}{\left(1 + \frac{2}{b/i}\right)\pi} \quad . \quad (B3)$$

For other values of ψ , such as $\pi/2$ and $3\pi/2$, no simple linear relations exist.

Blade tip on AS

Substitution of $x = 1$ in Eq. (8) leads to

$$\cos \psi - [\psi - (\frac{1}{2} - \frac{1}{b/i})\pi]\mu = 0 . \quad (B4)$$

For given μ , this equation results in ψ -values in Q1 which are close to $\pi/2$ (Figs. 3 and 5). The blade tip approaches the vortex in Q1 on its concave side (Fig. 1) and the point of intersection moves inward from the tip as ψ increases. See Section 6.3.2 for the rear side of the disc.

Rotor centre

For the intersection of the rotor centre with a tip vortex, $x = 0$ is substituted in Eq. (8). This results in

$$1 - [\psi - (1 - \frac{2}{b/i})\pi]\mu = 0 . \quad (B5)$$

For constant b/i , ψ decreases with increasing μ and decreasing b/i .

The condition $x = 0$ indicates either a case where the intersection point leaves the blade through the centre or where it starts its way along the blade. For even blade numbers, leaving one blade means passing to the diametrically opposite blade ($\Delta i = b/2$).

APPENDIX C

Division of advance ratio range 1

Advance ratio range 1a and $\bar{\mu}_a$

In the lowest part of μ -range 1 and after the intersection point of branch 1 has left the tip in Q4, a ψ -interval starts without intersection (Table 3, left). It ends because an intersection point moves on the blade at the rotor centre and then outward. In range 1a the next notable change in intersection occurs when the tip intersects again the vortex in Q1, resulting in two simultaneous intersections on the blade. These move towards each other during rotation until they coincide. The blade/vortex angle is then π . Thereafter no intersection occurs until the cycle starts again at the tip in Q1.

If now μ is increased, a critical situation occurs wherein the point with the radial tangent in Q1 reaches the tip. To find the corresponding critical advance ratio $\bar{\mu}_a$, $x = 1$ is substituted in Eq. (11), yielding

$$\bar{\mu}_a = \cos 2\bar{\psi}_a / \sin \bar{\psi}_a \quad (C1)$$

and by using Eq. (8)

$$2\bar{\psi}_a - \tan 2\bar{\psi}_a = -(1 + \frac{2}{b/i})\pi . \quad (C2)$$

Numerical results are presented in Table 6 and figures 5 and 7. The advance ratio $\bar{\mu}_a$ increases with b/i . The angle $\bar{\psi}_a$ is about 40° and almost independent of b/i .

In view of results obtained later-on for the other critical advance ratios, it is noted that only $\bar{\mu}_a$ for $b/i < 2$ disturbs the sequence of successive μ -ranges. The exception can be seen in Table 6 (left, bottom) and figure 7 (near origin): $\bar{\mu}_a$ for $b/i = 1$ is larger than $\bar{\mu}_b$. This has not been investigated any further.

Advance ratio range 1b and $\bar{\mu}_b$

This range differs from the lowest μ -range because the tangent situation in Q1 is absent (Table 3, middle). The characteristic pattern to be noted now is the ψ -interval in Q4 without intersection. Its upper limit is determined by the azimuth at which branch 2 starts at $x = 0$; this is given by Eq. (B5). If the advance ratio is increased, a critical value $\bar{\mu}_b$ is reached when this azimuth becomes equal to ψ at which the intersection point of branch 1 leaves the tip. See Eq. (B4) and Section 6.3.2. This leads to the condition

$$\cos \bar{\psi}_b = [\bar{\psi}_b - (\frac{3}{2} - \frac{1}{b/i})\pi] / [\bar{\psi}_b - (1 - \frac{2}{b/i})\pi] \quad , \quad (C3)$$

from which $\bar{\psi}_b$ can be calculated. The corresponding $\bar{\mu}_b$ (b/i) follows from Eq. (B5) for $x = 0$ or from Eq. (B4) for $x = 1$, both methods leading to identical values.

Numerical results are given in Table 6 and figures 5 and 7. The ratio $\bar{\mu}_b$ increases with b/i . The angle $\bar{\psi}_b$ in Q4 is about 290° .

Advance ratio range 1c

In the highest μ -range of range 1 (Table 3, right), the intersection point of branch 2 starts its way along the blade at a smaller ψ than at which the intersection of branch 1 leaves the tip. Therefore a ψ -range exists with two simultaneous intersections of the same vortex part on the blade.

The upper limit of range 1 is the first main critical advance ratio $\bar{\mu}$ and this is discussed in the second half of section 6.4.

APPENDIX D

Division of advance-ratio range 2

Advance ratio range 2a and $\bar{\mu}_a$

The lowest part of μ -range 2 (Table 4, left; $\bar{\mu} < \mu < \bar{\mu}_a$) is characterized by intersection branch 1 having a radial tangent in Q3 near the rotor centre.

As the blade rotates through Q3, an intersection point starts to move from the rotor centre outward, while the point coming from $x = 1$ in Q1 moves inward. In a small ψ -interval there are two simultaneous intersections. Both points meet in the inner region in Q3, with the blade tangent to the vortex.

After a ψ -interval without intersection, the blade becomes again tangent to the same vortex but now in the outer region. Further rotation leads to a separation into two simultaneously occurring intersection points on branch 2. The outer one moves outward and reaches the tip shortly afterwards; the inner point shifts inward more slowly, reaches x_m and thereafter moves outward to the tip in Q1 or Q4.

By increasing μ through this range, the radially tangent point of the branch 1 in Q3 moves inward. The upper limit $\bar{\mu}_a$ is defined as the value for which this point coincides with the rotor centre. The first interval with two simultaneous intersections has then vanished, but the interval for branch 2 still remains.

The corresponding $\bar{\psi}_a$ in Q3 and critical $\bar{\mu}_a$ follow from Eqs. (B5) and (11) with $x = 0$

$$\bar{\psi}_a - \tan \bar{\psi}_a = (1 - \frac{2}{b/i})\pi \quad , \quad (D1)$$

$$\bar{\mu}_a = \cotan \bar{\psi}_a \quad . \quad (D2)$$

Numerical results are presented in Table 6 and figure 7, which show the same general trend as for $\bar{\mu}_a$, $\bar{\mu}_b$ and $\bar{\mu}$.

As the characteristic events occur near the rotor centre and on the RS, it is anticipated that $\bar{\mu}_a$ is more of an academic than a practical interest.

Advance ratio range 2b and $\bar{\mu}_b$

The middle range of range 2 (Table 4) differs from the foregoing insofar that only the ψ -interval in Q4 with two simultaneous intersections of branch 2 has remained. For a further description of the intersection characteristics, reference is made to the preceding part of this Appendix.

The point of branch 2 with the radial tangent shifts outward as μ is increased until $x = 1$ at $\bar{\mu}_b$. This is the upper limit of this range, where ψ -intervals with two simultaneous intersections have disappeared.

The upper limit, in terms of $\bar{\mu}_b$ and $\bar{\psi}_b$, can be found from Eqs. (B4) and (11) with $x = 1$:

$$2\bar{\psi}_b - \tan 2\bar{\psi}_b = \left(3 - \frac{2}{b/i}\right)\pi, \quad (D3)$$

$$\bar{\mu}_b = \cos 2\bar{\psi}_b / \sin \bar{\psi}_b. \quad (D4)$$

The results of calculations are given in Table 6 and figure 7. The angle $\bar{\psi}_b$ varies only slightly around 305° .

Advance ratio range 2c

In the upper rest of range 2 (Table 4, right) there are no more ψ -intervals with two simultaneous intersections of the same vortex on the blade. The whole cycle consists of two intervals with alternately 0 and 1 intersection.

The upper limit of range 2 is the second main critical advance ratio $\bar{\mu}$ and this is discussed in section 6.5.

TABLE 1
 Characteristics of main advance-ratio ranges
 and main critical advance ratios

Range	1		2		3
Advance ratio	$0 < \mu < \bar{\mu}$	$\bar{\mu}$	$\bar{\mu} < \mu < \bar{\bar{\mu}}$	$\bar{\bar{\mu}}$	$\bar{\bar{\mu}} < \mu$
Quadrant for x_m	3 $1 > x_m > \bar{\mu}$	$\psi = 3\pi/2$ $x_m = \bar{\mu}$	4 $\bar{\mu} < x_m < 1$	4 $x_m = 1$ at $\bar{\psi}$	x_m absent (>1); only inner elements
Branch 1. Intersection starts at tip in Q1	moves inward until x_m ; then outward to leave blade tip in Q4		moves inward		
Branch 2. Intersection	starts at rotor centre and moves outward		starts in Q4, moves to x_m in Q4 and leaves blade at tip on aft side	reduced to $x = 1$ at $\bar{\psi}$	absent
Maximum number of sweeps behind disc over point in field along X-axis on AS	$\geq b + 3$	$b + 2$		$b + 1$ for $\mu < 2/\pi = 0.637$	

TABLE 2
The two main critical advance ratios
Characteristics of blade/vortex intersection patterns

Numbers around tip circle indicate number of simultaneous intersections on blade in azimuth interval

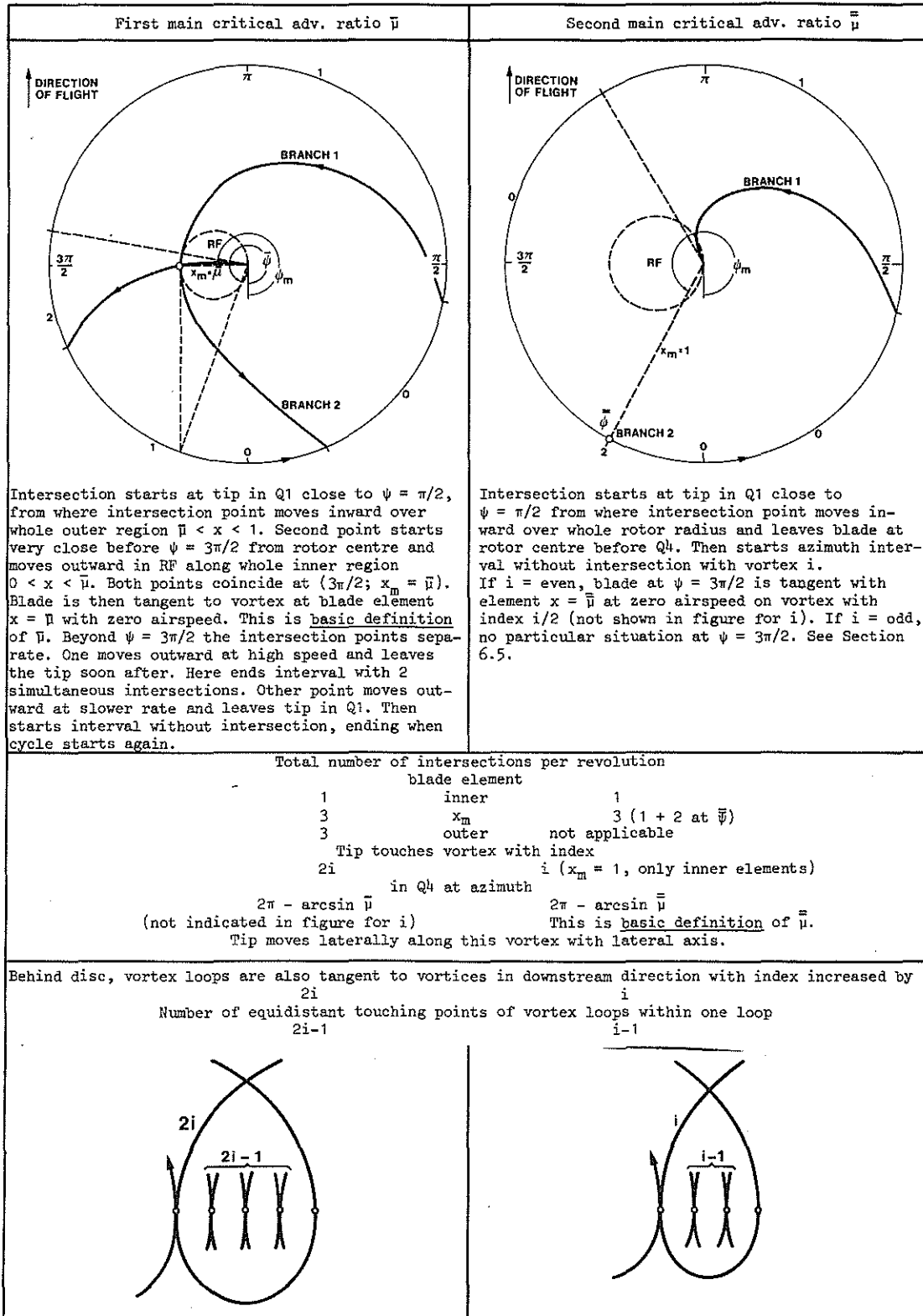


TABLE 3
Advance-ratio range 1
Characteristics of blade/vortex intersection patterns

Numbers around tip circle indicate number of simultaneous intersections on blade in azimuth interval

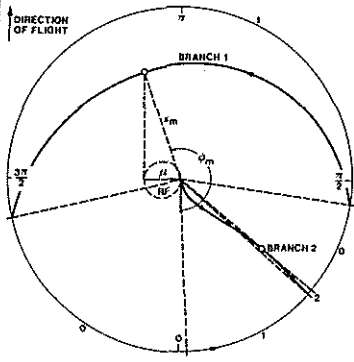
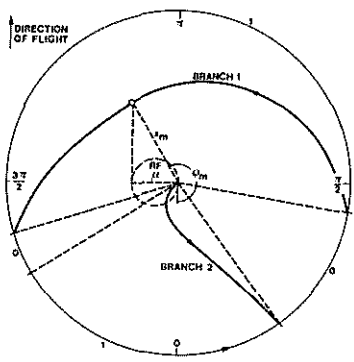
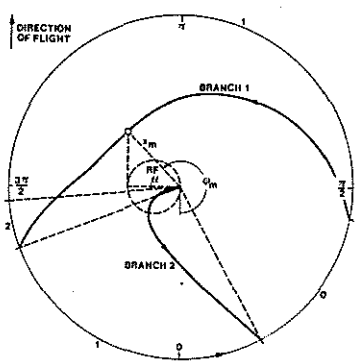
range 1a	ψ_a	range 1b	ψ_b	range 1c
	Radial tangent of branch 2 at ψ_a in Q1 for $x = 1$		Intersection leaves tip at ψ_b as branch 2 starts at rotor centre	
<p>Intersection starts at tip in Q1 close to $\psi = \pi/2$ from where intersection point moves inward along outer region ($x_m < x < 1$) of branch 1 until reaching x_m in Q3 at $Y = -\mu$. Blade element at x_m then moves laterally towards RS along vortex with lateral axis. Thereafter the intersection point moves outward and leaves tip in Q4. Outer elements have then experienced 2 intersections. Branch 2 of intersection points for older part of same vortex starts at rotor centre in Q1, Q4 or Q3 and has outer point at tip in Q1, contributing one intersection per revolution for all elements. Total intersections per revolution for inner elements 1, for outer elements 3.</p> <p>Intersection along branch 2 in Q1 starts at tip and moves inward, leading to 2 simultaneous intersections in this azimuth interval. At certain azimuth this point coincides with intersection point which came from rotor centre. Blade is then tangent to vortex.</p>		<p>Intersection along branch 2 leaves blade at tip</p>		<p>Large ψ-interval with 1 intersection ends because branch 2 starts in Q3 or Q4, leading to 2 simultaneous intersections. Thereafter intersection of branch 1 leaves tip in Q4, thus reducing intersections again to 1.</p>
First main critical advance ratio. $x_m = \bar{\psi}$ at $\psi = 3\pi/2$. Pattern in Table 2, left				

TABLE 4
Advance ratio range 2
Characteristics of blade/vortex intersection patterns

Numbers around tip circle indicate number of simultaneous intersections on blade in azimuth interval

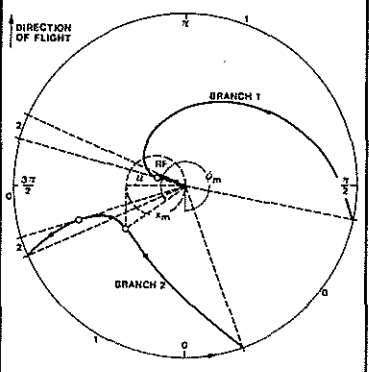
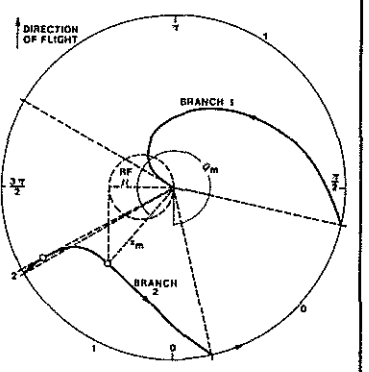
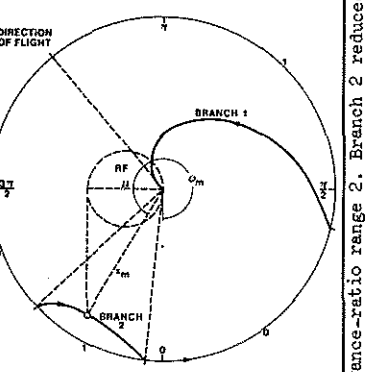
Ψ Intersection starts at tip in Q1 close to $\psi = \pi/2$ from where intersection point moves inward along branch 1 which has inner point at rotor centre. This contributes one intersection per revolution for all blade elements in Q1, Q2 or Q3. Branch 2 has two outer points at $x = 1$ in Q4+1 or Q4. Intersecting blade element with minimum radius occurs in Q4 at $Y = -\mu$ for $\psi = 2\pi - \arcsin \mu/x_m$. It moves laterally towards AS along lateral part of vortex. Intersection point thereafter moves outward and leaves blade at tip. This branch contributes 2 intersections/revolution, leading to total of 1 for inner and 3 for outer blade elements.					$\bar{\mu}$ Upper boundary of advance-ratio range 2. Branch 2 reduced to point at $\psi = 2\pi - \arcsin \bar{\mu}$; $x = 1$. See table 2, right.
$\bar{\mu}_a$ Lower boundary of advance-ratio range 2. Branches 1 and 2 meet at $\psi = 3\pi/2$; $x = \bar{\mu}$. See table 2, left.	range 2a 	$\bar{\mu}_b$ Radial tangent of branch 1 at $x = 0$	range 2b 	$\bar{\mu}_c$ Radial tangent of branch 2 at $x = 1$	range 2c 
Second intersection point on branch 1 moves outward from rotor centre in Q3 and coincides at slightly larger azimuth with inward moving point. Blade and intersection curve are then tangent to vortex at $x < x_m$ in RF.			Intersection point on branch 1 moves inward without radial tangent at $x > 0$ and leaves blade at rotor centre in Q2 or Q3. Azimuth interval with 2 intersections on blade has disappeared.		
Blade in Q4 at $x < 1$ becomes tangent to vortex. Further rotation leads to 2 intersection points. Outer point moves rapidly outward and leaves blade at tip in Q4. Inner point moves slowly inward.					
Intersection in Q4 occurs first at tip ($x = 1$), from where intersection point moves inward. Azimuth interval with 2 intersections in Q4 is absent					

TABLE 5
 Advance ratio range 3
 Characteristics of blade/vortex intersection pattern

Numbers around tip circle indicate number of simultaneous intersections on blade in azimuth interval

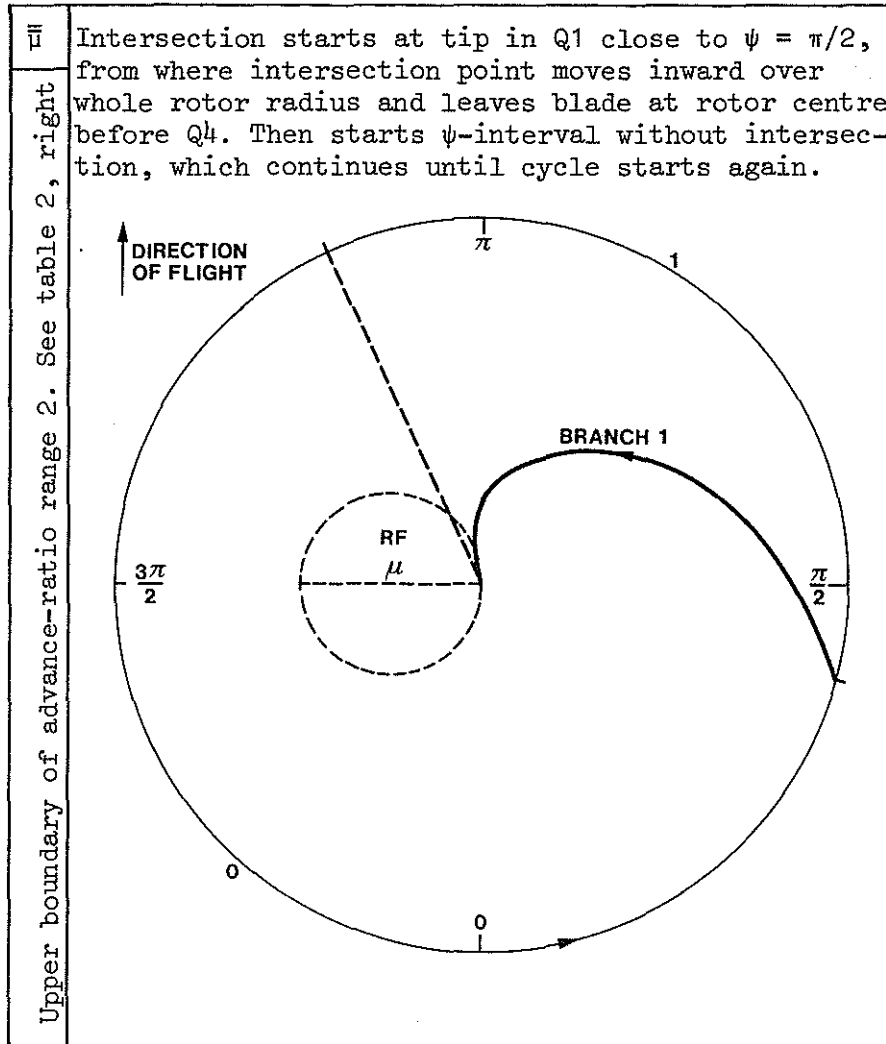


TABLE 6
The six critical advance ratios and corresponding
azimuth angles as a function of the ratio b/i
between the number of blades per rotor b and
the index i of a preceding blade

b/i	1	2	3	4	5	6	7
$\bar{\mu}(x_m=1)$	0.217	0.337	0.415	0.473	0.517	0.552	0.582
$\bar{\psi}$, deg	347.5	340.3	335.5	331.8	328.9	326.5	324.4
$\bar{\mu}_b$	0.171	0.278	0.354	0.412	0.457	0.494	0.525
$\bar{\psi}_b$, deg	311.3	308.7	306.8	305.2	303.8	302.7	301.8
$\bar{\mu}_a$	0.129	0.223	0.296	0.357	0.410	0.457	0.499
$\bar{\psi}_a$, deg	262.6	257.5	253.5	250.3	247.7	245.5	243.5
$\bar{\mu}(\min.x_m)$	0.128	0.217	0.284	0.337	0.379	0.415	0.446
$\bar{\psi}$, deg	352.6	347.5	343.5	340.3	337.7	335.5	333.5
$\bar{\mu}_b$	0.120	0.196	0.249	0.288	0.320	0.345	0.366
$\bar{\psi}_b$, deg	295.6	292.6	290.4	288.7	287.3	286.1	285.1
$\bar{\mu}_a$	0.135	0.194	0.228	0.249	0.264	0.275	0.283
$\bar{\psi}_a$, deg	42.4	41.3	40.7	40.4	40.1	39.9	39.8

TABLE 7

The two main critical advance ratios and corresponding azimuth angles for various combinations of number of blades per rotor, b , and index i of a preceding blade

i	μ ψ	i	$\bar{\mu}$ $\bar{\psi}$	Number of blades per rotor, b						
				1	2	3	4	5	6	7
		1	$\bar{\mu}_{b/1}$ $\bar{\psi}_{b/1}$	0.217 347.5	0.337 340.3	0.415 335.5	0.473 331.8	0.517 328.9	0.552 326.5	0.582 324.4
1	$\bar{\mu}_{b/1}$ $\bar{\psi}_{b/1}$	2	$\bar{\mu}_{b/2}$ $\bar{\psi}_{b/2}$	0.128 352.6	0.217 347.5	0.284 343.5	0.337 340.3	0.379 337.7	0.415 335.5	0.446 333.5
		3	$\bar{\mu}_{b/3}$ $\bar{\psi}_{b/3}$	0.091 354.8	0.161 350.7	0.217 347.5	0.264 344.7	0.303 342.4	0.337 340.3	0.386 338.5
2	$\bar{\mu}_{b/2}$ $\bar{\psi}_{b/2}$	4	$\bar{\mu}_{b/4}$ $\bar{\psi}_{b/4}$	0.071 355.9	0.128 352.6	0.176 349.8	0.217 347.5	0.253 345.4	0.284 343.5	0.312 341.8
		5	$\bar{\mu}_{b/5}$ $\bar{\psi}_{b/5}$	0.058 356.7	0.107 353.9	0.149 351.5	0.185 349.3	0.217 347.5	0.246 345.8	0.272 344.2
3	$\bar{\mu}_{b/3}$ $\bar{\psi}_{b/3}$	6	$\bar{\mu}_{b/6}$ $\bar{\psi}_{b/6}$	0.049 357.2	0.091 354.8	0.128 352.6	0.161 350.7	0.191 349.0	0.217 347.5	0.241 346.0

Note: b in subscript of μ and ψ refers here to number of blades per rotor; not to boundary between middle and highest ranges of advance ratio.